A STAGGERED DISCONTINUOUS GALERKIN METHOD FOR THE STOKES SYSTEM

HYEA HYUN KIM [*], ERIC T. CHUNG [†], AND CHAK SHING LEE[‡]

Abstract. Discontinuous Galerkin (DG) methods are a class of efficient tools for solving fluid flow problems. There are in literature many DG methods with great success. In this paper, a new staggered discontinuous Galerkin method for the Stokes system is developed and analyzed. The key feature of our method is that the discrete system preserves the structures of the continuous problem, which results from the use of our new staggered DG spaces. This also provides local and global conservation properties, which are desirable for fluid flow applications. The method is based on the first order mixed formulation involving pressure, velocity and velocity gradient. The velocity and velocity gradient are approximated by polynomials of the same degree while the choice of polynomial degree for pressure is flexible, namely the approximation degree for pressure can be chosen as either that of velocity or one degree lower than that of velocity. In any case, stability and optimal convergence of the method are proved. Moreover, a superconvergence result with respect to a discrete H^1-norm for the velocity is proved. Furthermore, a local postprocessing technique is proposed to improve divergence free property of the velocity approximation and it is proved that the postprocessed velocity retains the original accuracy and is weakly divergence free with respect to pressure test functions. Numerical results are included to validate our theoretical estimates and to present the ability of our method for capturing singular solutions.

Key words. staggered discontinuous Galerkin method, Stokes system, optimal convergence, conservation, superconvergence, divergence free, postprocessing

1. Introduction. Discontinuous Galerkin methods are getting their popularity in solving fluid flow problems. For example, in [11], the local discontinuous Galerkin (LDG) methods were developed for the Stokes system. These are stabilized mixed methods and a nonstandard inf-sup condition was proved. The methods give more flexibility in the choice of approximation spaces for the velocity and pressure. In particular, experimental results there showed that if polynomials of degree k and $k-1$ are used to approximate both velocity and pressure respectively, then the velocity converges with order $k+1$ in L^2 while the pressure converges with order k. When polynomials of the same degree k are used to approximate both velocity and pressure, the numerical solution still converge, but the order of convergence for the pressure does not improve because the L^2-error of the pressure also depends on the energy error of the velocity.

Due to their discontinuous nature, DG methods are also well-suited for hp-adaptivity; see [26] for a study on the mixed hp-DGFEM with the Q_k-Q_{k-1} elements and see also [27] in which corner singularities are treated and the authors derived exponential convergence for the methods used in [26] together with geometrically refined meshes.

For mixed DG methods, the numerical solutions normally satisfy the divergence-free constraint weakly, as is the case for the method presented in this paper. Methodologies producing globally divergence-free approximations can be found in [10, 8]

Recently, in [9], the authors analyzed hybridizable discontinuous Galerkin (HDG) methods applied to the stationary Stokes flow. In their work all the unknowns (velocity, velocity gradient and pressure) are approximated by piecewise polynomials of degree at most k. On the other hand their elements are totally discontinuous across element interfaces, in contrast to our staggered continuity setting which will be described in detail. The performance of their methods hinges on the choice of

a stabilization tensor which connects the numerical traces. It was shown that the L^2-errors of all the numerical solutions converge with the optimal order $k + 1$, which is a significant improvement over other finite element methods in the context of incompressible fluid flow problems. Moreover, a postprocessing technique is proposed and the postprocessed velocity is exactly divergence free.

In this paper, we develop a staggered discontinuous Galerkin formulation for the Stokes problem by using piecewise polynomials which are partially continuous across inter-element boundaries. The idea of staggered grid in the computation of fluid flow has been applied successfully in the context of finite difference framework, see for example [23] and [3], and the finite volume framework, see for example [2], in order to avoid the addition of artificial viscosity. Staggered finite volume formulation is also widely used for wave propagation problems [14, 15]. Our staggered DG formulation generalizes staggered finite difference/finite volume methods, retains the local conservation property and provides a higher order numerical scheme for fluid flow applications on triangular meshes.

In our formulation, the Stokes problem is rewritten into a system of first order equations by using three variables: velocity gradient, velocity and pressure. All these variables are approximated with piecewise polynomials of the same degree. We emphasize that the velocity gradient only acts as an auxiliary variable and will not be solved in the resulting linear system. The continuity of polynomials for velocity gradient, velocity and pressure are staggered on the inter-element boundaries. In other words, on the common part of two elements, one of them is continuous and the other can be discontinuous. The use of these staggered variables gives a discretization that preserves the structures of the continuous problem. In particular, the discrete gradient and divergence operators are adjoint to each other. Also, the discrete Laplacian operator is symmetric and positive definite without the need of penalization.

The staggered continuity property naturally gives inter-element flux term in our discontinuous Galerkin formulation in contrast to other discontinuous Galerkin methods, in which numerical fluxes or penalty parameters have to be carefully chosen. Similar to [9], we prove that the L^2-errors of all solutions are of order $k + 1$ when piecewise polynomials of order up to k are used, and we prove in addition that the velocity converges with the optimal order k with respect to the energy norm. Even though our method gives a larger linear system and geometrically more complicated supports of basis function, it provides a promising alternative to [9] in the sense that our method is easy to implement without the need to specify a stabilization tensor and it is straightforward to apply existing domain decomposition preconditioners for fast solutions, since our resulting algebraic system preserves the structure of the Stokes system and pressure functions are decoupled across the triangle boundaries, see also [25]. Another feature of our method is that the approximation degree of pressure can be taken one order lower than velocity, without affecting the accuracy of the velocity and the stability of the method, in order to reduce the computational cost. Moreover, a superconvergence result is obtained, namely, the error of the velocity in the energy norm is $k + 1$ when the error is computed as the difference between the numerical solution and the interpolant into the new DG space.

In addition, we propose a local postprocessing technique in order to enhance the divergence free property of our numerical solution. The postprocessed velocity is globally H(div)-conforming, retains the original accuracy and satisfies a local divergence free condition. Note that, in contrast to [9] which gives a pointwise divergence free condition, the postprocessed velocity considered in this paper is divergence free in a stronger integral sense. In particular, the elementwise integral of the product of the divergence and any test function in the pressure space is zero. The computation of this postprocessed velocity is performed locally, and is thus very efficient. Furthermore, in order to demonstrate that our method is capable of capturing the corner singularities, we test our method with a singular function in the L-shaped domain. The computational experiments in Section 6 show promising results and the performance of our method is comparable to the ones in [24].

In this article, we consider the Stokes problem with homogeneous boundary condition:

$$
\begin{aligned}
-\boldsymbol{\Delta u} + \nabla p &= \boldsymbol{f} \ \text{ in } \Omega, \\
\operatorname{div} \boldsymbol{u} &= 0 \ \text{ in } \Omega, \\
\boldsymbol{u} &= 0 \ \text{ on } \partial\Omega,
\end{aligned}
\tag{1.1}
$$

where $\boldsymbol{u} = (u_1, u_2)$, $\boldsymbol{f} = (f_1, f_2)$ and $\int_\Omega p \, dx = 0$. We introduce the auxiliary variables

$$
\boldsymbol{w} = \nabla u_1, \quad \boldsymbol{z} = \nabla u_2.
\tag{1.2}
$$

Then (1.1) can be reformulated as

$$
\begin{aligned}
-\operatorname{div} \boldsymbol{w} + p_x &= f_1 \ \text{ in } \Omega, \\
-\operatorname{div} \boldsymbol{z} + p_y &= f_2 \ \text{ in } \Omega, \\
\operatorname{div} \boldsymbol{u} &= 0 \ \text{ in } \Omega, \\
\boldsymbol{u} &= 0 \ \text{ on } \partial\Omega,
\end{aligned}
\tag{1.3}
$$

together with the constraint that $\int_\Omega p \, dx = 0$. The numerical methods in this paper are based on the first order system of (1.2) and (1.3).

The paper is organized as follows. In Section 2, the construction of the staggered discontinuous Galerkin discretization is given in detail. The mathematical theory of the method is presented in Section 3 and Section 4. In particular, the inf-sup condition, stability, convergence and superconvergence of the method are rigorously analyzed. In Section 5, we will present the local postprocessing technique, and in Section 6, numerical results are shown.

2. Staggered discontinuous Galerkin discretization. We will derive our staggered DG method based on triangular meshes. The construction of the meshes, the corresponding finite element spaces and the discrete variational forms will be presented in the following sections. We will focus our attention to the two-dimensional setting for simplicity. Extension of our method to the three-dimensional case follows essentially along the same lines, see [19] for the construction of three dimensional staggered grid.

2.1. Staggered DG spaces on triangular meshes. Following [12, 16, 17, 18], we first define the triangulation. For rectangular mesh, we can use the idea in [13]. Suppose the domain Ω is triangulated by a set of triangles without hanging nodes. We use the notation $\mathcal{F}_u$ to denote the set of all edges in this triangulation and use the notation $\mathcal{F}_u^0$ to denote the subset of all interior edges in $\mathcal{F}_u$. For each triangle, we take an interior point ν, and divide this triangle into three subtriangles by connecting the point ν to the three vertices of the triangle. The union of these three subtriangles is called $\mathcal{S}(\nu)$. We introduce the notation $\mathcal{N}$ to denote the set of all such interior points ν. We use the notation $\mathcal{F}_p$ to denote all new edges generated by the subdivision of triangles and use $\mathcal{T}$ to denote the triangulation after subdivision. Note that, the interior points ν should be chosen so that $\mathcal{T}$ satisfies the standard shape regularity assumption. In addition, $\mathcal{F} = \mathcal{F}_u \cup \mathcal{F}_p$ denotes the set of all edges of $\mathcal{T}$ and $\mathcal{F}^0 = \mathcal{F}_u^0 \cup \mathcal{F}_p$ denotes the set of all interior edges of $\mathcal{T}$.

For each edge $e \in \mathcal{F}_u$, we let $\mathcal{R}(e)$ be the union of the two triangles sharing the edge e. When e is a boundary edge, $\mathcal{R}(e)$ is the only triangle having the edge e. FIG. 2.1 illustrates these definitions. We remark that this kind of triangulation is also quite useful in other types of methods and applications. For example, in [1], it is used to prove some stability results for the quadratic velocity/linear pressure conforming finite elements. In [22], it is used to prove that weak symmetry implies strong symmetry in some discontinuous Galerkin formulation for the elasticity equations.
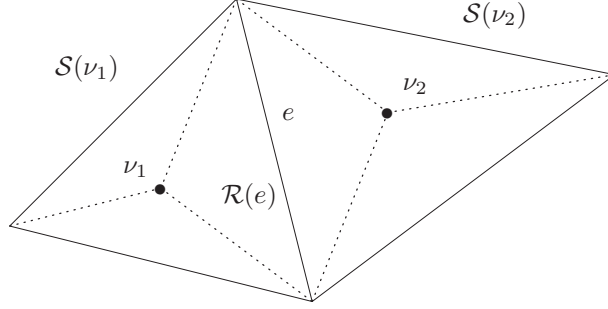
FIG. 2.1. *An illustration of the staggered mesh in two dimensions.*

We will also define a unit normal vector $\boldsymbol{n}_e$ on each edge e in $\mathcal{F}$ by the following way. If $e \in \mathcal{F} \backslash \mathcal{F}^0$ is a boundary edge, then we define $\boldsymbol{n}_e$ as the unit normal vector of e pointing outside of Ω. If $e \in \mathcal{F}^0$ is an interior face, then we fix $\boldsymbol{n}_e$ as one of the two possible unit normal vectors on e. When it is clear that which edge we are considering, we will use $\boldsymbol{n}$ instead of $\boldsymbol{n}_e$ to simplify the notations.

We will now discuss the finite element spaces. Let $k \geq 0$ be a non-negative integer. Let $\tau \in \mathcal{T}$ and $e \in \mathcal{F}$. We define $P^k(\tau)$ and $P^k(e)$ as the spaces of polynomials of degree up to k on τ and e, respectively. We then define the following:

Locally $H^1(\Omega)$-conforming finite element space for velocity

$$U^h = \{v \ : \ v|_\tau \in P^k(\tau); \ \tau \in \mathcal{T}; \ v \text{ is continuous over } e \in \mathcal{F}_u^0; \ v|_{\partial\Omega} = 0\}. \tag{2.1}$$

Notice that, if $v \in U^h$, then $v|_{\mathcal{R}(e)} \in H^1(\mathcal{R}(e))$ for each edge $e \in \mathcal{F}_u$. Furthermore, the condition $v|_{\partial\Omega} = 0$ is equivalent to $v|_e = 0$ for all $e \in \mathcal{F}_u \backslash \mathcal{F}_u^0$ since $\mathcal{F}_u$ contains all the boundary edges. We also define the following degrees of freedom.

(UD1). For each edge $e \in \mathcal{F}_u^0$, we have

$$\phi_e(v) := \int_e v p_k \, d\sigma$$

for all $p_k \in P^k(e)$.

(UD2). For each $\tau \in \mathcal{T}$, we have

$$\phi_\tau(v) := \int_\tau v p_{k-1} \, dx$$

for all $p_{k-1} \in P^{k-1}(\tau)$.

In this paper, we use the notation $|\mathcal{S}|$ to represent the number of elements in the set $\mathcal{S}$. By [17], any function v in the locally $H^1(\Omega)$-conforming finite element space U^h is uniquely determined by the degrees of freedom (UD1)-(UD2).

In the space U^h we define the following norms

$$\|u\|_X^2 := \int_\Omega u^2 \, dx + \sum_{e \in \mathcal{F}_u^0} h_e \int_\kappa u^2 \, d\sigma, \tag{2.2}$$

$$\|u\|_Z^2 := \int_\Omega |\nabla_h u|^2 \, dx + \sum_{e \in \mathcal{F}_p} h_e^{-1} \int_e [u]^2 \, d\sigma, \tag{2.3}$$

4

where we remark that the integral of $\nabla_h u$ in (2.3) is defined element by element. Here we recall that, by definition, $u \in U^h$ is continuous on each edge e in the set $\mathcal{F}_u^0$ while it can be discontinuous on each edge e in the set $\mathcal{F}_p$. We say $\|u\|_X$ is the discrete L^2-norm of u and $\|u\|_Z$ is the discrete H^1-norm of u. In the above definition, the jump $[u]$ over e is defined as

$$[u] = u_1 \boldsymbol{n} - u_2 \boldsymbol{n}$$

where $u_i = u|_{\tau_i}$, e is the common edge of two triangles τ_1 and τ_2, and $\boldsymbol{n}$ is the unit normal to the edge e.

Now, we define the following:

Locally $H(\mathbf{div}; \Omega)$-conforming finite element space

$$W^h = \{\boldsymbol{w} \,:\, \boldsymbol{w}|_\tau \in P^k(\tau)^2;\, \tau \in \mathcal{T};\, \boldsymbol{w} \cdot \boldsymbol{n} \text{ is continuous over } e \in \mathcal{F}_p\}. \tag{2.4}$$

Notice that, if $\boldsymbol{w} \in W^h$, then $\boldsymbol{w}|_{\mathcal{S}(\nu)} \in H(\mathrm{div}; \mathcal{S}(\nu))$ for each $\nu \in \mathcal{N}$. We also define the following degrees of freedom.

(WD1). For each $e \in \mathcal{F}_p$, we have

$$\psi_e(\boldsymbol{w}) := \int_e \boldsymbol{w} \cdot \boldsymbol{n} \, p_k \, d\sigma$$

for all $p_k \in P^k(e)$.

(WD2). For each $\tau \in \mathcal{T}$, we have

$$\psi_\tau(\boldsymbol{w}) := \int_\tau \boldsymbol{w} \cdot \boldsymbol{p}_{k-1} \, dx$$

for all $\boldsymbol{p}_{k-1} \in P^{k-1}(\tau)^2$.

By [17], any function $\boldsymbol{w}$ in the locally $H(\mathrm{div}; \Omega)$-conforming finite element space W^h is uniquely determined by the degrees of freedom (WD1)-(WD2).

In the space W^h, we define the following norms

$$\|\boldsymbol{w}\|_{X'}^2 := \int_\Omega |\boldsymbol{w}|^2 \, dx + \sum_{e \in \mathcal{F}_p} h_e \int_e (\boldsymbol{w} \cdot \boldsymbol{n})^2 \, d\sigma, \tag{2.5}$$

$$\|\boldsymbol{w}\|_{Z'}^2 := \int_\Omega (\mathrm{div}_h \, \boldsymbol{w})^2 \, dx + \sum_{e \in \mathcal{F}_u^0} h_e^{-1} \int_e [\boldsymbol{w} \cdot \boldsymbol{n}]^2 \, d\sigma, \tag{2.6}$$

where we remark that the integral of $\mathrm{div}_h \, \boldsymbol{w}$ in (2.6) is defined elementwise. Note that the discrete norm $\| \cdot \|_{X'}$ is equivalent to the L^2 norm, see [17]. More precisely, there exists a constant $k_1 > 0$, independent of h, such that

$$k_1 \|\boldsymbol{w}\|_{X'} \leq \|\boldsymbol{w}\|_{0,\Omega} \leq \|\boldsymbol{w}\|_{X'} \quad \forall \boldsymbol{w} \in W^h \tag{2.7}$$

where $\| \cdot \|_{0,\Omega}$ denotes the L^2-norm defined on Ω. Here we recall that, by definition, $\boldsymbol{w} \in W^h$ has continuous normal component on each edge in $e \in \mathcal{F}_p$. We say $\|\boldsymbol{w}\|_{X'}$ is the discrete L^2-norm of $\boldsymbol{w}$ and $\|\boldsymbol{w}\|_{Z'}$ is the discrete $H(\mathrm{div}; \Omega)$-norm of $\boldsymbol{w}$. In the above definition, the jump $[\boldsymbol{w} \cdot \boldsymbol{n}]$ over e is defined as

$$[\boldsymbol{w} \cdot \boldsymbol{n}] = \boldsymbol{w}_1 \cdot \boldsymbol{n} - \boldsymbol{w}_2 \cdot \boldsymbol{n},$$

5

where $\boldsymbol{w}_i = \boldsymbol{w}|_{\tau_i}$, e is the common edge of two triangles τ_1 and τ_2, and $\boldsymbol{n}$ is a unit normal to the edge e.

We denote the numerical approximation of $\boldsymbol{u} = (u_1, u_2)$ by $\boldsymbol{u}_h = (u_{h,1}, u_{h,2})$ and the numerical approximation of $\boldsymbol{w} = \nabla u_1$ and $\boldsymbol{z} = \nabla u_2$ by $\boldsymbol{w}_h$ and $\boldsymbol{z}_h$, respectively. Each component of the numerical approximation $\boldsymbol{u}_h$ is in the space U^h, while $\boldsymbol{w}_h$ and $\boldsymbol{z}_h$ are in the space W^h. Hence, we are seeking a numerical solution $\boldsymbol{u}_h$ in the product space $[U^h]^2$, for which we define the energy norm by

$$\|\boldsymbol{v}_h\|_h := \sqrt{\|v_{h,1}\|_Z^2 + \|v_{h,2}\|_Z^2}.$$

As for the pressure p, we find the numerical solution p_h in another function space P^h which is defined as:

Locally $H^1(\Omega)$-conforming finite element space for pressure

$$P^h = \{q \; : \; q|_\tau \in P^k(\tau); \; \tau \in \mathcal{T}; \; q \text{ is continuous over } e \in \mathcal{F}_p; \; \int_\Omega q \, dx = 0\}.$$

Note that this is a finite dimensional subspace of $L_0^2(\Omega) := \{q \in L^2(\Omega)| \int_\Omega q \, dx = 0\}$. We equip this space with the following norm

$$\|q\|_P^2 = \int_\Omega q^2 \, dx + \sum_{e \in \mathcal{F}_p} h_e \int_e q^2 \, d\sigma. \tag{2.8}$$

Similar to the discrete norm $\| \cdot \|_{X'}$, this norm is also equivalent to the standard L^2-norm:

$$k_2\|q\|_P \le \|q\|_{0,\Omega} \le \|q\|_P, \;\; \forall q \in P^h. \tag{2.9}$$

Moreover, we observe that functions in P^h and U^h are continuous on different edges belonging to $\mathcal{F}_p$ and $\mathcal{F}_u^0$, respectively. For the analysis in the following sections, we relax the average constraint on P^h and define

$$\widehat{P}^h = \{q \; : \; q|_\tau \in P^k(\tau); \; \tau \in \mathcal{T}; \; q \text{ is continuous over } e \in \mathcal{F}_p\}. \tag{2.10}$$

REMARK 1. *For the Stokes problem, the lower order polynomial $P^{k-1}(\tau)$ is commonly used for pressure approximation to achieve inf-sup stability. In our approach, we can use $P^{k-1}(\tau)$ for the pressure and prove that L^2 errors for the pressure converge with the order k as in the standard finite element methods for the Stokes problem. Using the higher order approximation $P^k(\tau)$ for the pressure, we can still obtain the inf-sup stability and prove that L^2 errors converge with the order $k + 1$. The same result was proved in the work [9] where only the convergence of L^2 errors was analyzed. In our work, we also provide energy-norm error estimate for the velocity approximation.*

2.2. Discrete problem. We will derive the discrete problem in our DG formulation starting from the system of first order equations in (1.2) and (1.3). Multiplying the first equation of (1.2) by $\boldsymbol{\psi} \in W^h$ and integrating over $\mathcal{S}(\nu)$ for $\nu \in \mathcal{N}$, we have

$$\int_{\mathcal{S}(\nu)} \boldsymbol{w} \cdot \boldsymbol{\psi} \, dx = -\int_{\mathcal{S}(\nu)} u_1 \nabla \cdot \boldsymbol{\psi} \, dx + \int_{\partial \mathcal{S}(\nu)} u_1 \boldsymbol{\psi} \cdot \boldsymbol{n} \, d\sigma. \tag{2.11}$$

Similarly, multiplying the second equation of (1.2) by $\boldsymbol{\psi} \in W^h$ and integrating over $\mathcal{S}(\nu)$ for $\nu \in \mathcal{N}$, we have

$$\int_{\mathcal{S}(\nu)} \boldsymbol{z} \cdot \boldsymbol{\psi} \, dx = -\int_{\mathcal{S}(\nu)} u_2 \nabla \cdot \boldsymbol{\psi} \, dx + \int_{\partial \mathcal{S}(\nu)} u_2 \boldsymbol{\psi} \cdot \boldsymbol{n} \, d\sigma. \tag{2.12}$$

Multiplying the first equation of (1.3) by $\phi_1 \in U^h$ and integrating over $\mathcal{R}(e)$ for $e \in \mathcal{F}_u^0$, we have

$$\int_{\mathcal{R}(e)} \boldsymbol{w} \cdot \nabla\phi_1 \, dx - \int_{\partial\mathcal{R}(e)} (\boldsymbol{w} \cdot \boldsymbol{n})\phi_1 \, d\sigma - \int_{\mathcal{R}(e)} p(\phi_1)_x + \int_{\partial\mathcal{R}(e)} p\phi_1 n_1 \, d\sigma = \int_{\mathcal{R}(e)} f_1\phi_1 \, dx. \quad (2.13)$$

Similarly, multiplying the second equation of (1.3) by $\phi_2 \in U^h$ and integrating over $\mathcal{R}(e)$ for $e \in \mathcal{F}_u^0$, we have

$$\int_{\mathcal{R}(e)} \boldsymbol{z} \cdot \nabla\phi_2 \, dx - \int_{\partial\mathcal{R}(e)} (\boldsymbol{z} \cdot \boldsymbol{n})\phi_2 \, d\sigma - \int_{\mathcal{R}(e)} p(\phi_2)_y \, dx + \int_{\partial\mathcal{R}(e)} p\phi_2 n_2 \, d\sigma = \int_{\mathcal{R}(e)} f_2\phi_2 \, dx. \quad (2.14)$$

Finally, for $q \in P^h$,

$$\int_{\mathcal{S}(\nu)} (\operatorname{div}\boldsymbol{u}) q \, dx = 0$$

and integration by parts again gives that

$$-\int_{\mathcal{S}(\nu)} \boldsymbol{u} \cdot \nabla q \, dx + \int_{\partial\mathcal{S}(\nu)} (\boldsymbol{u} \cdot \boldsymbol{n})q \, d\sigma = 0. \quad (2.15)$$

Equations (2.11), (2.12), (2.13), (2.14) and (2.15) give our new method. We emphasize here that locally, functions in U^h, W^h and P^h are all polynomials of degree k. Summing those equations over all $\mathcal{R}(e)$ and $\mathcal{S}(\nu)$, our new staggered discontinuous Galerkin method for (1.1) is obtained:

Find $(\boldsymbol{u}_h, \boldsymbol{w}_h, \boldsymbol{z}_h, p_h) \in [U^h]^2 \times W^h \times W^h \times P^h$ such that

$$
\begin{aligned}
B_h(\boldsymbol{w}_h, \phi_1) + B_h(\boldsymbol{z}_h, \phi_2) + b_h^*(p_h, \boldsymbol{\Phi}) &= (\boldsymbol{f}, \boldsymbol{\Phi})_{0,\Omega} & \forall \boldsymbol{\Phi} = (\phi_1, \phi_2) \in [U^h]^2, \\
B_h^*(u_{h,1}, \boldsymbol{\psi}_1) &= (\boldsymbol{w}_h, \boldsymbol{\psi}_1)_{0,\Omega} & \forall \boldsymbol{\psi}_1 \in W^h, \\
B_h^*(u_{h,2}, \boldsymbol{\psi}_2) &= (\boldsymbol{z}_h, \boldsymbol{\psi}_2)_{0,\Omega} & \forall \boldsymbol{\psi}_2 \in W^h, \\
b_h(\boldsymbol{u}_h, q) &= 0 & \forall q \in P^h,
\end{aligned}
\quad (2.16)
$$

where bilinear forms $B_h(\boldsymbol{w}_h, v)$ and $B_h^*(u_h, \boldsymbol{z})$ are defined as

$$
\begin{aligned}
B_h(\boldsymbol{w}_h, v) &= \int_\Omega \boldsymbol{w}_h \cdot \nabla_h v \, dx - \sum_{e \in \mathcal{F}_p} \int_e \boldsymbol{w}_h \cdot \boldsymbol{n} \, [v] \, d\sigma, \\
B_h^*(u_h, \boldsymbol{z}) &= -\int_\Omega u_h \operatorname{div}_h \boldsymbol{z} \, dx + \sum_{e \in \mathcal{F}_u^0} \int_e u_h \, [\boldsymbol{z} \cdot \boldsymbol{n}] \, d\sigma.
\end{aligned}
\quad (2.17)
$$

and the bilinear forms $b_h^*(p_h, \boldsymbol{v})$ and $b_h(\boldsymbol{u}_h, q)$ are defined as

$$
\begin{aligned}
b_h^*(p_h, \boldsymbol{v}) &= -\int_\Omega p_h \operatorname{div}_h \boldsymbol{v} \, dx + \sum_{e \in \mathcal{F}_p} \int_e p_h[\boldsymbol{v} \cdot \boldsymbol{n}] \, d\sigma, \\
b_h(\boldsymbol{u}_h, q) &= \int_\Omega \boldsymbol{u}_h \cdot \nabla q \, dx - \sum_{e \in \mathcal{F}_u^0} \int_e \boldsymbol{u}_h \cdot \boldsymbol{n}[q] \, d\sigma.
\end{aligned}
\quad (2.18)
$$

Those two bilinear forms in (2.17) possess some properties that will be used throughout this paper. To begin with, by [17], we have

$$B_h(\boldsymbol{w}, v) = B_h^*(v, \boldsymbol{w}) \quad (2.19)$$

7

for all $v \in U_h$ and $\boldsymbol{w} \in W^h$. This means the bilinear forms B_h and B_h^* are adjoint to each other. Secondly, it can be shown by the Cauchy-Schwarz inequality that

$$
\begin{aligned}
|B_h(\boldsymbol{w}, v)| &\leq \|\boldsymbol{w}\|_{X'} \|v\|_Z, \\
|B_h^*(v, \boldsymbol{w})| &\leq \|v\|_X \|\boldsymbol{w}\|_{Z'},
\end{aligned}
\tag{2.20}
$$

for all $(\boldsymbol{w}, v) \in W^h \times U^h$. Hence, both B_h and B_h^* are continuous with respect to suitable discrete norms. Moreover, the following inf-sup condition holds (see [17]): there exists a positive constant β, independent of h, such that

$$
\beta \|v\|_Z \leq \sup_{\boldsymbol{w} \in W^h} \frac{B_h^*(v, \boldsymbol{w})}{\|\boldsymbol{w}\|_{X'}}.
\tag{2.21}
$$

Lastly, there exist operators $I : H_0^1(\Omega) \to U^h$ and $J : H(\mathrm{div}; \Omega) \to W^h$ such that for $u \in H_0^1(\Omega)$ and $\boldsymbol{w} \in H(\mathrm{div}; \Omega)$,

$$
\begin{aligned}
B_h^*(Iu - u, \boldsymbol{\psi}) &= 0 \quad \forall \boldsymbol{\psi} \in W^h, \\
B_h(J\boldsymbol{w} - \boldsymbol{w}, \phi) &= 0 \quad \forall \phi \in U^h,
\end{aligned}
\tag{2.22}
$$

and when $u \in H^{k+1}(\Omega)$ and $\boldsymbol{w} \in [H^{k+1}(\Omega)]^2$

$$
\|Iu - u\|_Z \leq Ch^k |u|_{H^{k+1}(\Omega)}, \quad \|J\boldsymbol{w} - \boldsymbol{w}\|_{0,\Omega} \leq Ch^{k+1} |\boldsymbol{w}|_{[H^{k+1}(\Omega)]^2}
\tag{2.23}
$$

where we only require the domain Ω to satisfy standard assumptions so that classical interpolation theories hold. Note that, the proof of the second estimate in (2.23) does not involve any duality argument. The bilinear forms B_h and B_h^* will actually take care of the discretization for the Laplacian operator.

For the bilinear forms in (2.18) related to the pressure term, we observe that

$$
b_h^*(q, \boldsymbol{v}) = b_h(\boldsymbol{v}, q)
\tag{2.24}
$$

and again from the Cauchy-Schwarz inequality it is continuous

$$
|b_h(\boldsymbol{v}, q)| \leq \frac{1}{k_2} \|\boldsymbol{v}\|_h \|q\|_{0,\Omega}, \forall (\boldsymbol{v}, q) \in [U^h]^2 \times P^h.
\tag{2.25}
$$

In addition, we need to prove inf-sup condition for the bilinear form $b_h(\boldsymbol{v}, q)$ to proceed error estimates for our DG approximation.

3. Inf-sup condition. This section is devoted to the proof of an inf-sup condition for the bilinear form b_h, which is crucial in proving the convergence and stability of the numerical scheme.

THEOREM 3.1. *There exists a constant γ, independent of h, such that*

$$
\inf_{p \in P^h \setminus \{0\}} \sup_{\boldsymbol{u} \in [U^h]^2 \setminus \{\boldsymbol{0}\}} \frac{b_h(\boldsymbol{u}, p)}{\|\boldsymbol{u}\|_h \|p\|_{0,\Omega}} \geq \gamma.
\tag{3.1}
$$

Proof. Let $p \in P^h \setminus \{0\}$ be arbitrary. By definition, $p \in L_0^2(\Omega)$, so there exists $\boldsymbol{u} = (u_1, u_2) \in [H_0^1(\Omega)]^2$, see for example [21], such that

$$
-\int_\Omega \mathrm{div}\, \boldsymbol{u}\, p\, dx = \|p\|_{0,\Omega}^2
$$

$$
\|\boldsymbol{u}\|_{1,\Omega} \leq C\|p\|_{0,\Omega}.
\tag{3.2}
$$

Next, we define an interpolation operator $\Pi_h : H_0^1(\Omega) \to U^h$ such that every $v \in H_0^1(\Omega)$, for each edge $e \in \mathcal{F}_u^0$,

$$\int_e \Pi_h v \, q \, d\sigma = \int_e v q \, d\sigma, \ \forall q \in P^k(e), \tag{3.3}$$

and for each $\tau \in \mathcal{T}$,

$$\int_\tau \Pi_h v \, q \, dx = \int_\tau v q \, dx, \ \forall q \in P^{k-1}(\tau). \tag{3.4}$$

Note that this operator coincides with the operator I defined in (2.22). Therefore Π_h is stable, see [17], in the sense that

$$\|\Pi_h v\|_Z \leq C\|v\|_{1,\Omega}. \tag{3.5}$$

Let $\boldsymbol{\Pi_h u} = (\Pi_h u_1, \Pi_h u_2)$ for $\boldsymbol{u} = (u_1, u_2)$. Note that $\nabla_h p$ is a piecewise polynomial of degree $k - 1$, it follows that

$$
\begin{aligned}
-\int_\Omega \operatorname{div} \boldsymbol{u} \, p \, dx &= -\sum_{\nu \in \mathcal{N}} \int_{\mathcal{S}(\nu)} \operatorname{div} \boldsymbol{u} \, p \, dx = -\sum_{\nu \in \mathcal{N}} \left(\int_{\partial \mathcal{S}(\nu)} \boldsymbol{u} \cdot \boldsymbol{n} \, p \, d\sigma - \int_{\mathcal{S}(\nu)} \boldsymbol{u} \cdot \nabla p \, dx \right) \\
&= \sum_{\nu \in \mathcal{N}} \int_{\mathcal{S}(\nu)} \boldsymbol{u} \cdot \nabla p \, dx - \sum_{e \in \mathcal{F}_u^0} \int_e \boldsymbol{u} \cdot \boldsymbol{n} \, [p] \, d\sigma \\
&= \sum_{\nu \in \mathcal{N}} \int_{\mathcal{S}(\nu)} \boldsymbol{\Pi_h u} \cdot \nabla p \, dx - \sum_{e \in \mathcal{F}_u^0} \int_e \boldsymbol{\Pi_h u} \cdot \boldsymbol{n} \, [p] \, d\sigma \\
&= b_h(\boldsymbol{\Pi_h u}, p),
\end{aligned} \tag{3.6}
$$

where we have used (3.3) and (3.4) in the second to last step. Combining (3.2) and (3.6), we have

$$b_h(\boldsymbol{\Pi_h u}, p) = -\int_\Omega \operatorname{div} \boldsymbol{u} \, p \, dx = \|p\|_{0,\Omega}^2.$$

Also, by (3.2), (3.5) and the definition of $\|\cdot\|_h$, we know that

$$\|\boldsymbol{\Pi_h u}\|_h \leq C\|\boldsymbol{u}\|_{1,\Omega} \leq C\|p\|_{0,\Omega}.$$

Hence, the result follows.

$\square$

REMARK 2. *The interpolation operator Π_h defined in the proof of Theorem 3.1 actually satisfies the Fortin property. It is well-known that the existence of such an operator leads to the* inf-sup *condition of b_h, cf. [4].*

4. Abstract error analysis. We are going to derive error bounds for the numerical solution obtained from the proposed scheme. The following estimates are useful.

LEMMA 4.1. *Let $(\phi, \boldsymbol{v}) \in U^h \times W^h$ be such that*

$$(\boldsymbol{v}, \boldsymbol{\psi})_{0,\Omega} = B_h^*(\phi, \boldsymbol{\psi}) \quad \forall \boldsymbol{\psi} \in W^h. \tag{4.1}$$

Then we have

$$\|\boldsymbol{v}\|_{0,\Omega} \leq \frac{1}{k_1} \|\phi\|_Z,$$

$$\|\phi\|_Z \leq \frac{1}{\beta} \|\boldsymbol{v}\|_{0,\Omega},$$

9

where the constants k_1 and β are the ones in the norm equivalence (2.7) and inf-sup *condition for B_h^* (2.21), respectively.*

Proof. It follows from (4.1), the continuity of B_h^* (2.20) and the norm equivalence (2.7) that

$$\|\boldsymbol{v}\|_{0,\Omega} = \sup_{\boldsymbol{\psi}\in W^h\setminus\{\boldsymbol{0}\}} \frac{(\boldsymbol{v},\boldsymbol{\psi})_{0,\Omega}}{\|\boldsymbol{\psi}\|_{0,\Omega}} \le \frac{1}{k_1} \sup_{\boldsymbol{\psi}\in W^h\setminus\{\boldsymbol{0}\}} \frac{B_h^*(\phi,\boldsymbol{\psi})}{\|\boldsymbol{\psi}\|_{X'}} \le \frac{1}{k_1}\|\phi\|_Z.$$

Similarly,

$$\|\phi\|_Z \le \frac{1}{\beta} \sup_{\boldsymbol{\psi}\in W^h\setminus\{\boldsymbol{0}\}} \frac{B_h^*(\phi,\boldsymbol{\psi})}{\|\boldsymbol{\psi}\|_{X'}} \le \frac{1}{\beta} \sup_{\boldsymbol{\psi}\in W^h\setminus\{\boldsymbol{0}\}} \frac{(\boldsymbol{v},\boldsymbol{\psi})_{0,\Omega}}{\|\boldsymbol{\psi}\|_{0,\Omega}} \le \frac{1}{\beta}\|\boldsymbol{v}\|_{0,\Omega}.$$

So the result follows.

$\square$

Next, we show the well-posedness of the discrete problem.

PROPOSITION 4.2. *The discrete problem (2.16) admits a unique solution $(\boldsymbol{u}_h, \boldsymbol{w}_h, \boldsymbol{z}_h, p_h) \in [U^h]^2 \times W^h \times W^h \times P^h$. Moreover, it is stable in the sense that*

$$
\begin{aligned}
\|\boldsymbol{u}_h\|_h &\le \frac{C_p}{\beta^2}\|\boldsymbol{f}\|_{0,\Omega}, \\
\|\boldsymbol{u}_h\|_{0,\Omega} &\le \frac{C_p^2}{\beta^2}\|\boldsymbol{f}\|_{0,\Omega}, \\
\|p_h\|_{0,\Omega} &\le \frac{C_p}{\gamma}\big(1 + \frac{\sqrt{2}}{k_1^2\beta^2}\big)\|\boldsymbol{f}\|_{0,\Omega}, \\
\|\boldsymbol{w}_h\|_{0,\Omega} + \|\boldsymbol{z}_h\|_{0,\Omega} &\le \frac{\sqrt{2}C_p}{k_1\beta^2}\|\boldsymbol{f}\|_{0,\Omega}.
\end{aligned}
\tag{4.2}
$$

Here, k_1, β, γ are the constants in the norm equivalence (2.7), inf-sup conditions (2.21), (3.1), respectively. C_p is a constant that stems from the Poincaré-Friedrichs inequality for piecewise-H^1 functions. All these constants are independent of the mesh size h.

Proof. Note that if (4.2) holds, the existence and uniqueness of the discrete solution follow immediately. So all we need to show is the bounds (4.2). From the second and third equations of (2.16), we know that the pairs $(u_{h,1}, \boldsymbol{w}_h)$ and $(u_{h,2}, \boldsymbol{z}_h)$ satisfy the hypothesis of Lemma 4.1. Hence, we have

$$
\begin{aligned}
\|\boldsymbol{w}_h\|_{0,\Omega} &\le \frac{1}{k_1}\|u_{h,1}\|_Z, \quad \|\boldsymbol{z}_h\|_{0,\Omega} \le \frac{1}{k_1}\|u_{h,2}\|_Z, \\
\|u_{h,1}\|_Z &\le \frac{1}{\beta}\|\boldsymbol{w}_h\|_{0,\Omega}, \quad \|u_{h,2}\|_Z \le \frac{1}{\beta}\|\boldsymbol{z}_h\|_{0,\Omega}.
\end{aligned}
\tag{4.3}
$$

Then, by setting $(\boldsymbol{\Phi}, \boldsymbol{\psi}_1, \boldsymbol{\psi}_2, q) = (\boldsymbol{u}_h, \boldsymbol{w}_h, \boldsymbol{z}_h, p_h)$ as the test functions in (2.16) and using the discrete adjoint property (2.19) and (2.24) we get

$$\|\boldsymbol{w}_h\|_{0,\Omega}^2 + \|\boldsymbol{z}_h\|_{0,\Omega}^2 = (\boldsymbol{f}, \boldsymbol{u}_h)_{0,\Omega}.$$

Now it follows from the last two inequalities of (4.3) and the Poincaré-Friedrichs inequality for piecewise H^1-functions, see [7], that

$$\beta^2\|\boldsymbol{u}_h\|_h^2 \le \|\boldsymbol{w}_h\|_{0,\Omega}^2 + \|\boldsymbol{z}_h\|_{0,\Omega}^2 \le \|\boldsymbol{f}\|_{0,\Omega}\|\boldsymbol{u}_h\|_{0,\Omega} \le C_p\|\boldsymbol{f}\|_{0,\Omega}\|\boldsymbol{u}_h\|_h, \tag{4.4}$$

10

where C_p depends only on the shape regularity of the mesh $\mathcal{T}$. Thus, we have derived the first bound. Applying the Poincaré-Friedrichs inequality to $\boldsymbol{u}_h$ again yields

$$\|\boldsymbol{u}_h\|_{0,\Omega} \le C_p\|\boldsymbol{u}_h\|_h \le \frac{C_p^2}{\beta^2}\|\boldsymbol{f}\|_{0,\Omega}.$$

Also, by the first two inequalities of (4.3) we get

$$\|\boldsymbol{w}_h\|_{0,\Omega} + \|\boldsymbol{z}_h\|_{0,\Omega} \le \frac{\sqrt{2}}{k_1}\|\boldsymbol{u}_h\|_h \le \frac{\sqrt{2}C_p}{k_1\beta^2}\|\boldsymbol{f}\|_{0,\Omega}.$$

Lastly, the inf-sup condition for b_h (3.1), the discrete adjoint property (2.24), and the continuity of B_h (2.20) implies that

$$\begin{aligned}
\|p_h\|_{0,\Omega} &\le \frac{1}{\gamma}\sup_{\boldsymbol{\Phi}\in[U^h]^2\backslash\{\mathbf{0}\}}\frac{b_h(\boldsymbol{\Phi},p_h)}{\|\boldsymbol{\Phi}\|_h}\\
&= \frac{1}{\gamma}\sup_{\boldsymbol{\Phi}\in[U^h]^2\backslash\{\mathbf{0}\}}\frac{(\boldsymbol{f},\boldsymbol{\Phi})_{0,\Omega} - B_h(\boldsymbol{w}_h,\phi_1) - B_h(\boldsymbol{z}_h,\phi_2)}{\|\boldsymbol{\Phi}\|_h}\\
&\le \frac{1}{\gamma}\Big(C_p\|\boldsymbol{f}\|_{0,\Omega} + \|\boldsymbol{w}_h\|_{X'} + \|\boldsymbol{z}_h\|_{X'}\Big)\\
&\le \frac{C_p}{\gamma}\big(1 + \frac{\sqrt{2}}{k_1^2\beta^2}\big)\|\boldsymbol{f}\|_{0,\Omega}.
\end{aligned}$$

$\square$

Using the continuity and inf-sup conditions of the bilinear forms B_h, B_h^* and b_h, together with Lemma 4.1 we can establish the convergence of the proposed scheme.

THEOREM 4.3. *Suppose* $(\boldsymbol{u},\boldsymbol{w},\boldsymbol{z},p)$ *and* $(\boldsymbol{u}_h,\boldsymbol{w}_h,\boldsymbol{z}_h,p_h)$ *satisfy (1.2), (1.3) and (2.16), respectively. Then the following error bounds hold*

$$\|\boldsymbol{u}-\boldsymbol{u}_h\|_h \le \|\boldsymbol{u}-I\boldsymbol{u}\|_h + \frac{1}{\beta^2}\inf_{q\in P^h}\|p-q\|_P + \frac{2}{k_1\beta^2}\Big(\|\boldsymbol{w}-J\boldsymbol{w}\|_{0,\Omega} + \|\boldsymbol{z}-J\boldsymbol{z}\|_{0,\Omega}\Big),$$

$$\|p-p_h\|_P \le \Big(1 + \frac{1}{k_2\gamma}\big(1 + \frac{\sqrt{2}}{k_1^2\beta^2}\big)\Big)\inf_{q\in P^h}\|p-q\|_P + \frac{2}{k_1 k_2\gamma}\big(1 + \frac{\sqrt{2}}{k_1^2\beta^2}\big)\Big(\|\boldsymbol{w}-J\boldsymbol{w}\|_{0,\Omega} + \|\boldsymbol{z}-J\boldsymbol{z}\|_{0,\Omega}\Big),$$

$$\|\boldsymbol{w}-\boldsymbol{w}_h\|_{0,\Omega} + \|\boldsymbol{z}-\boldsymbol{z}_h\|_{0,\Omega} \le \frac{\sqrt{2}}{k_1\beta^2}\inf_{q\in P^h}\|p-q\|_P + \Big(1 + \frac{2\sqrt{2}}{k_1^2\beta^2}\Big)\Big(\|\boldsymbol{w}-J\boldsymbol{w}\|_{0,\Omega} + \|\boldsymbol{z}-J\boldsymbol{z}\|_{0,\Omega}\Big). \quad (4.5)$$

Here, k_1,β,γ *are same as the ones in Proposition 4.2 and* k_2 *is the constant in the norm equivalence (2.9). Again, all these constants are independent of the mesh size* h.

Proof. Consider the element $I\boldsymbol{u} = (Iu_1, Iu_2) \in [U^h]^2$, where $\boldsymbol{u} = (u_1, u_2)$ is the exact solution to (1.2), (1.3) and Iu_i is defined in (2.22). We recall that this interpolation $I\boldsymbol{u}$ coincides with $\boldsymbol{\Pi_h u}$ in the proof of Theorem 3.1. Hence, by (3.6), we have

$$b_h(I\boldsymbol{u},q) = -\int_\Omega \operatorname{div}\boldsymbol{u}\, q\, dx = 0$$

for all $q \in P^h$. We take $\tilde{\boldsymbol{w}}, \tilde{\boldsymbol{z}} \in W^h$ such that

$$(\tilde{\boldsymbol{w}},\boldsymbol{\psi})_{0,\Omega} = B_h^*(Iu_1,\boldsymbol{\psi}) \quad \forall\boldsymbol{\psi}\in W^h,$$
$$(\tilde{\boldsymbol{z}},\boldsymbol{\psi})_{0,\Omega} = B_h^*(Iu_2,\boldsymbol{\psi}) \quad \forall\boldsymbol{\psi}\in W^h.$$

11

Now observe that, by using (2.13), (2.14), the first equation in (2.16), and the discrete adjoint property (2.24), we have

$$B_h(\boldsymbol{w} - \boldsymbol{w}_h, \phi_1) + B_h(\boldsymbol{z} - \boldsymbol{z}_h, \phi_2) + b_h(\boldsymbol{\Phi}, p - p_h) = 0, \qquad \forall \boldsymbol{\Phi} = (\phi_1, \phi_2) \in [U^h]^2. \tag{4.6}$$

Then taking $\boldsymbol{\Phi} = I\boldsymbol{u} - \boldsymbol{u}_h$, we obtain

$$\begin{aligned}
&B_h(\tilde{\boldsymbol{w}} - \boldsymbol{w}_h, Iu_1 - u_{h,1}) + B_h(\tilde{\boldsymbol{z}} - \boldsymbol{z}_h, Iu_2 - u_{h,2}) \\
=&B_h(\tilde{\boldsymbol{w}} - \boldsymbol{w}, Iu_1 - u_{h,1}) + B_h(\tilde{\boldsymbol{z}} - \boldsymbol{z}, Iu_2 - u_{h,2}) + b_h(I\boldsymbol{u} - \boldsymbol{u}_h, p_h - p) \\
=&B_h(\tilde{\boldsymbol{w}} - J\boldsymbol{w}, Iu_1 - u_{h,1}) + B_h(\tilde{\boldsymbol{z}} - J\boldsymbol{z}, Iu_2 - u_{h,2}) + b_h(I\boldsymbol{u} - \boldsymbol{u}_h, q - p),
\end{aligned} \tag{4.7}$$

where J is the interpolation operator defined in (2.22) and we have used the fact that $b_h(I\boldsymbol{u} - \boldsymbol{u}_h, q) = 0$ for all $q \in P^h$ in the last equality. It then follows from the continuity of B_h and b_h, and norm equivalence in (2.7) and (2.9) that

$$\begin{aligned}
&B_h(\tilde{\boldsymbol{w}} - J\boldsymbol{w}, Iu_1 - u_{h,1}) + B_h(\tilde{\boldsymbol{z}} - J\boldsymbol{z}, Iu_2 - u_{h,2}) + b_h(I\boldsymbol{u} - \boldsymbol{u}_h, q - p), \\
\leq&\|\tilde{\boldsymbol{w}} - J\boldsymbol{w}\|_{X'}\|Iu_1 - u_{h,1}\|_Z + \|\tilde{\boldsymbol{z}} - J\boldsymbol{z}\|_{X'}\|Iu_2 - u_{h,2}\|_Z + \|p - q\|_P\|I\boldsymbol{u} - \boldsymbol{u}_h\|_h \\
\leq&\frac{1}{k_1}\|\tilde{\boldsymbol{w}} - J\boldsymbol{w}\|_{0,\Omega}\|Iu_1 - u_{h,1}\|_Z + \frac{1}{k_1}\|\tilde{\boldsymbol{z}} - J\boldsymbol{z}\|_{0,\Omega}\|Iu_2 - u_{h,2}\|_Z + \|p - q\|_P\|I\boldsymbol{u} - \boldsymbol{u}_h\|_h.
\end{aligned} \tag{4.8}$$

On the other hand, using the second and the third equations in (2.16), we have

$$\begin{aligned}
(\tilde{\boldsymbol{w}} - \boldsymbol{w}_h, \boldsymbol{\psi})_{0,\Omega} = B_h^*(Iu_1 - u_{h,1}, \boldsymbol{\psi}) \ \ \forall \boldsymbol{\psi} \in W^h, \\
(\tilde{\boldsymbol{z}} - \boldsymbol{z}_h, \boldsymbol{\psi})_{0,\Omega} = B_h^*(Iu_2 - u_{h,2}, \boldsymbol{\psi}) \ \ \forall \boldsymbol{\psi} \in W^h.
\end{aligned} \tag{4.9}$$

Then, using the discrete adjoint property (2.19) and Lemma 4.1 we have

$$\begin{aligned}
&B_h(\tilde{\boldsymbol{w}} - \boldsymbol{w}_h, Iu_1 - u_{h,1}) + B_h(\tilde{\boldsymbol{z}} - \boldsymbol{z}_h, Iu_2 - u_{h,2}) \\
=&B_h^*(Iu_1 - u_{h,1}, \tilde{\boldsymbol{w}} - \boldsymbol{w}_h) + B_h^*(Iu_2 - u_{h,2}, \tilde{\boldsymbol{z}} - \boldsymbol{z}_h) \\
=&\|\tilde{\boldsymbol{w}} - \boldsymbol{w}_h\|_{0,\Omega}^2 + \|\tilde{\boldsymbol{z}} - \boldsymbol{z}_h\|_{0,\Omega}^2 \\
\geq&\beta^2\Big(\|Iu_1 - u_{h,1}\|_Z^2 + \|Iu_2 - u_{h,2}\|_Z^2\Big).
\end{aligned} \tag{4.10}$$

Combining (4.7), (4.8) and (4.10), we have

$$\|I\boldsymbol{u} - \boldsymbol{u}_h\|_h \leq \frac{1}{k_1\beta^2}\|\tilde{\boldsymbol{w}} - J\boldsymbol{w}\|_{0,\Omega} + \frac{1}{k_1\beta^2}\|\tilde{\boldsymbol{z}} - J\boldsymbol{z}\|_{0,\Omega} + \frac{1}{\beta^2}\|p - q\|_P. \tag{4.11}$$

It is worth noting that for all $\boldsymbol{\psi} \in W^h$,

$$(\tilde{\boldsymbol{w}}, \boldsymbol{\psi})_{0,\Omega} = B_h^*(Iu_1, \boldsymbol{\psi}) = B_h^*(u_1, \boldsymbol{\psi}) = (\boldsymbol{w}, \boldsymbol{\psi})_{0,\Omega},$$

which means that $\tilde{\boldsymbol{w}}$ is the L^2 projection of $\boldsymbol{w}$ into the space W^h. Because $J\boldsymbol{w} \in W^h$, the following estimate holds:

$$\|\tilde{\boldsymbol{w}} - \boldsymbol{w}\|_{0,\Omega} \leq \|J\boldsymbol{w} - \boldsymbol{w}\|_{0,\Omega}$$

and therefore

$$\|\tilde{\boldsymbol{w}} - J\boldsymbol{w}\|_{0,\Omega} \leq \|\tilde{\boldsymbol{w}} - \boldsymbol{w}\|_{0,\Omega} + \|\boldsymbol{w} - J\boldsymbol{w}\|_{0,\Omega} \leq 2\|\boldsymbol{w} - J\boldsymbol{w}\|_{0,\Omega}. \tag{4.12}$$

Similarly, $\|\tilde{\boldsymbol{z}} - J\boldsymbol{z}\|_{0,\Omega} \le 2\|\boldsymbol{z} - J\boldsymbol{z}\|_{0,\Omega}$. Hence, from (4.11) we have

$$\|I\boldsymbol{u} - \boldsymbol{u}_h\|_h \le \frac{2}{k_1\beta^2}\|\boldsymbol{w} - J\boldsymbol{w}\|_{0,\Omega} + \frac{2}{k_1\beta^2}\|\boldsymbol{z} - J\boldsymbol{z}\|_{0,\Omega} + \frac{1}{\beta^2}\|p - q\|_P. \qquad (4.13)$$

By the triangle inequality, we can obtain the first error bound in (4.5).

To get the estimate for the L^2 error of the velocity gradient, we note that by (4.9) and Lemma 4.1, we have

$$k_1\Big(\|\tilde{\boldsymbol{w}} - \boldsymbol{w}_h\|_{0,\Omega} + \|\tilde{\boldsymbol{z}} - \boldsymbol{z}_h\|_{0,\Omega}\Big) \le \|Iu_1 - u_{h,1}\|_Z + \|Iu_2 - u_{h,2}\|_Z \le \sqrt{2}\|I\boldsymbol{u} - \boldsymbol{u}_h\|_h. \qquad (4.14)$$

Then the last estimate in (4.5) is a direct consequence of (4.13), (4.14) and the inequalities

$$\|\boldsymbol{w} - \boldsymbol{w}_h\|_{0,\Omega} \le \|\boldsymbol{w} - \tilde{\boldsymbol{w}}\|_{0,\Omega} + \|\tilde{\boldsymbol{w}} - \boldsymbol{w}_h\|_{0,\Omega} \le \|\boldsymbol{w} - J\boldsymbol{w}\|_{0,\Omega} + \|\tilde{\boldsymbol{w}} - \boldsymbol{w}_h\|_{0,\Omega},$$
$$\|\boldsymbol{z} - \boldsymbol{z}_h\|_{0,\Omega} \le \|\boldsymbol{z} - \tilde{\boldsymbol{z}}\|_{0,\Omega} + \|\tilde{\boldsymbol{z}} - \boldsymbol{z}_h\|_{0,\Omega} \le \|\boldsymbol{z} - J\boldsymbol{z}\|_{0,\Omega} + \|\tilde{\boldsymbol{z}} - \boldsymbol{z}_h\|_{0,\Omega}.$$

For the error estimate of $\|p - p_h\|_{0,\Omega}$, we note that the inf-sup condition implies that

$$\gamma\|p_h - q\|_{0,\Omega} \le \sup_{\boldsymbol{v} \in [U^h]^2\setminus\{\boldsymbol{0}\}} \frac{b_h(\boldsymbol{v}, p_h - q)}{\|\boldsymbol{v}\|_h}.$$

Moreover, (4.6) yields

$$b_h(\boldsymbol{v}, p_h - q) = b_h(\boldsymbol{v}, p - q) + B_h(\boldsymbol{w} - \boldsymbol{w}_h, v_1) + B_h(\boldsymbol{z} - \boldsymbol{z}_h, v_2)$$
$$= b_h(\boldsymbol{v}, p - q) + B_h(J\boldsymbol{w} - \boldsymbol{w}_h, v_1) + B_h(J\boldsymbol{z} - \boldsymbol{z}_h, v_2),$$

for all $\boldsymbol{v} = (v_1, v_2) \in U^h$. As both b_h and B_h are continuous, we then obtain that

$$\gamma\|p_h - q\|_{0,\Omega} \le \|p - q\|_P + \|J\boldsymbol{w} - \boldsymbol{w}_h\|_{X'} + \|J\boldsymbol{z} - \boldsymbol{z}_h\|_{X'}$$
$$\le \|p - q\|_P + \frac{1}{k_1}\Big(\|J\boldsymbol{w} - \tilde{\boldsymbol{w}}\|_{0,\Omega} + \|J\boldsymbol{z} - \tilde{\boldsymbol{z}}\|_{0,\Omega} + \|\tilde{\boldsymbol{w}} - \boldsymbol{w}_h\|_{0,\Omega} + \|\tilde{\boldsymbol{z}} - \boldsymbol{z}_h\|_{0,\Omega}\Big)$$
$$\le \|p - q\|_P + \frac{2}{k_1}\Big(\|J\boldsymbol{w} - \boldsymbol{w}\|_{0,\Omega} + \|J\boldsymbol{z} - \boldsymbol{z}\|_{0,\Omega}\Big) + \frac{\sqrt{2}}{k_1^2}\|I\boldsymbol{u} - \boldsymbol{u}_h\|_h$$
$$\le \Big(1 + \frac{\sqrt{2}}{k_1^2\beta^2}\Big)\|p - q\|_P + \frac{2}{k_1}\Big(1 + \frac{\sqrt{2}}{k_1^2\beta^2}\Big)\Big(\|J\boldsymbol{w} - \boldsymbol{w}\|_{0,\Omega} + \|J\boldsymbol{z} - \boldsymbol{z}\|_{0,\Omega}\Big),$$

where we have used (4.12) and (4.14) in the third inequality, and used (4.13) in the last inequality. Now the second error estimate in (4.5) follows again from triangle inequality and the norm equivalence (2.9). $\qquad \square$

To obtain the L^2-error estimate for the velocity, we can prove the following bound by a standard duality argument, see [6, Chapter II. 7.6 Aubin-Nitsche Lemma], when $\boldsymbol{u} \in [H^{1+\sigma}(\Omega)]^2$ and $p \in H^\sigma(\Omega)$ with $\sigma \ge 1$:

$$\begin{aligned}
&\|I\boldsymbol{u} - \boldsymbol{u}_h\|_{0,\Omega} \\
&= \sup_{\boldsymbol{g} \in [L^2(\Omega)]^2} \frac{(\boldsymbol{g}, I\boldsymbol{u} - \boldsymbol{u}_h)_{0,\Omega}}{\|\boldsymbol{g}\|_{0,\Omega}} \\
&\le C(k_1)h\left(\|I\boldsymbol{u} - \boldsymbol{u}\|_h + \|\boldsymbol{u} - \boldsymbol{u}_h\|_h + \|J\boldsymbol{w} - \boldsymbol{w}_h\|_{0,\Omega} + \|J\boldsymbol{z} - \boldsymbol{z}_h\|_{0,\Omega} + \|p - p_h\|_P\right),
\end{aligned} \qquad (4.15)$$

13

where $C(k_1)$ is a constant depending on k_1 but not depending on the mesh size h. We note that k_1 is the same constant as in Theorem 4.3. Combining the above bound with the estimates in Theorem 4.3 and with the triangle inequality, we obtain the L^2-error estimate for the velocity:

THEOREM 4.4. *For $\boldsymbol{u}$, p and $\boldsymbol{u}_h$ in Theorem 4.3, the following L^2-error estimate holds when $\boldsymbol{u} \in [H^{1+\sigma}(\Omega)]^2$ and $p \in H^\sigma(\Omega)$ with $\sigma \geq 1$,*

$$\|\boldsymbol{u} - \boldsymbol{u}_h\|_{0,\Omega}$$

$$\leq \|\boldsymbol{u} - I\boldsymbol{u}\|_{0,\Omega} + C(k_1, k_2, \beta, \gamma)h \left(\|\boldsymbol{u} - I\boldsymbol{u}\|_h + \inf_{q \in P^h} \|p - q\|_P + \|\boldsymbol{w} - J\boldsymbol{w}\|_{0,\Omega} + \|\boldsymbol{z} - J\boldsymbol{z}\|_{0,\Omega} \right),$$

where $C(k_1, k_2, \beta, \gamma)$ denotes a constant depending on k_1, k_2, β, and γ but not depending on the mesh size h. Those constants k_1, k_2, β, and γ are same as ones in Theorem 4.3.

In Theorems 4.3 and 4.4, we can take $q = \pi_h p \in P^h$ where π_h is the standard conforming finite element interpolation operator for the triangulation $\mathcal{T}$. Then we have (c.f. [20])

$$\|p - \pi_h p\|_{0,\Omega} \leq Ch^{k+1}|p|_{H^{k+1}(\Omega)} \quad \text{and} \quad \|p - \pi_h p\|_{L^2(e)} \leq Ch^{k+\frac{1}{2}}|p|_{H^{k+1}(\tau)}$$

where $e \in \partial\tau$ and $\tau \in \mathcal{T}$. By taking into account the approximation properties of the space U^h and W^h in (2.23) as well as the definition of the P-norm on the space P^h, an explicit error bound follows easily from Theorems 4.3 and 4.4. We state it as a corollary.

COROLLARY 4.5. *Let $(\boldsymbol{u}, \boldsymbol{w}, \boldsymbol{z}, p)$ and $(\boldsymbol{u}_h, \boldsymbol{w}_h, \boldsymbol{z}_h, p_h)$ be as in Theorem 4.3 with the additional assumptions that $(\boldsymbol{u}, p) \in [H^{1+\sigma}(\Omega)]^2 \times H^\sigma(\Omega)$. We have*

$$\begin{aligned}
&\|\boldsymbol{u} - \boldsymbol{u}_h\|_h \leq Ch^{\min\{k,\sigma\}} \left(\|\boldsymbol{u}\|_{[H^{\min\{k,\sigma\}+1}(\Omega)]^2} + \|p\|_{H^{\min\{k,\sigma\}}(\Omega)} \right), \\
&\|\boldsymbol{u} - \boldsymbol{u}_h\|_{0,\Omega} \leq Ch^{\min\{k+1,1+\sigma\}} \left(\|\boldsymbol{u}\|_{[H^{\min\{k,\sigma\}+1}(\Omega)]^2} + \|p\|_{H^{\min\{k,\sigma\}}(\Omega)} \right), \ (only \ for \ \sigma \geq 1) \\
&\|p - p_h\|_{0,\Omega} \leq Ch^{\min\{k+1,\sigma\}} \left(\|\boldsymbol{u}\|_{[H^{\min\{k+2,\sigma+1\}}(\Omega)]^2} + \|p\|_{H^{\min\{k+1,\sigma\}}(\Omega)} \right), \\
&\|\boldsymbol{w} - \boldsymbol{w}_h\|_{0,\Omega} + \|\boldsymbol{z} - \boldsymbol{z}_h\|_{0,\Omega} \leq Ch^{\min\{k+1,\sigma\}} \left(\|\boldsymbol{u}\|_{[H^{\min\{k+2,\sigma+1\}}(\Omega)]^2} + \|p\|_{H^{\min\{k+1,\sigma\}}(\Omega)} \right).
\end{aligned} \tag{4.16}$$

where the constant C is independent of h.

We remark that the condition $\sigma \geq 1$ is required for the duality argument used to prove (4.15), and hence the second estimate in (4.16). Note that, this condition holds when the domain is a convex polygon.

Moreover, from (4.13) and the above approximation properties, we obtain the following superconvergence result for the velocity.

COROLLARY 4.6. *Under the same assumptions in Corollary 4.5, we have the following superconvergence estimate:*

$$\|I\boldsymbol{u} - \boldsymbol{u}_h\|_h \leq Ch^{\min\{k+1,\sigma\}} \left(\|\boldsymbol{u}\|_{[H^{\min\{k+2,\sigma+1\}}(\Omega)]^2} + \|p\|_{H^{\min\{k+1,\sigma\}}(\Omega)} \right) \tag{4.17}$$

where the constant C is independent of h.

We remark that all the above stability and convergence theories as well as the inf-sup condition for the bilinear form b_h are valid if the approximation space for the pressure is replaced by the following space

$$\tilde{P}^h = \{q \in \ | \ q|_\tau \in P^{k-1}(\tau); \ \tau \in \mathcal{T}; \ q \text{ is continuous over } e \in \mathcal{F}_p; \ \int_\Omega q \ dx = 0\}$$

14

which is one order lower than P^h. In particular, (3.6) holds when $p \in \tilde{P}^h$. The resulting method is then similar to the classical finite element method. We also note that the lower order pressure does not affect the accuracy for the velocity and keeps it as the same order $k + 1$ in the L^2 norm and k in the energy norm, see the bound in Theorem 4.4 and also the first bound in Theorem 4.3.

5. Postprocessing and local conservation. It is well-known that local conservation is an important property for the Stokes flow. From (2.16) and the discrete adjoint property (2.24), we see that our numerical solution $\boldsymbol{u}_h$ satisfies the following local divergence-free condition

$$-\int_{\mathcal{S}(\nu)} q \operatorname{div}_h \boldsymbol{u}_h \, dx + \sum_{e \in \mathcal{E}(\nu)} \int_e q[\boldsymbol{u}_h \cdot \boldsymbol{n}] \, d\sigma = 0, \quad \forall q \in \widehat{P}^h|_{\mathcal{S}(\nu)} \tag{5.1}$$

where $\mathcal{E}(\nu)$ is the set of all edges having the vertex ν. Note that, in the above argument, we have used the fact that the last equation of (2.16) also holds for all $q \in \widehat{P}^h$, see (2.10) for the definition of $\widehat{P}^h$. While (5.1) provides some form of local conservation, it may not be accurate enough for some cases, see numerical illustration in the following section.

To improve the local conservation, we will introduce a local postprocessing technique. Let τ be a given triangle and $RT_k(\tau)$ be the Raviart-Thomas element of degree k defined on the triangle τ. We then define a vector $\boldsymbol{r}_{h,\tau} \in RT_k(\tau)$ by the following degrees of freedom:

$$\int_e p_k \, \boldsymbol{r}_{h,\tau} \cdot \boldsymbol{m} \, d\sigma = \int_e \frac{1}{2}[\boldsymbol{u}_h \cdot \boldsymbol{n}] \, p_k \, d\sigma, \quad \forall p_k \in P^k(e), \quad e \subset \partial\tau,$$
$$\int_\tau \boldsymbol{p}_{k-1} \cdot \boldsymbol{r}_{h,\tau} \, dx = 0, \quad \forall \boldsymbol{p}_{k-1} \in P^{k-1}(\tau)^2 \tag{5.2}$$

where $\boldsymbol{m}$ is the outward unit normal vector defined on $\partial\tau$. We remark that $\boldsymbol{n}$ is a fixed normal direction on the edge e. Notice that, in (5.2), $[\boldsymbol{u}_h \cdot \boldsymbol{n}] = 0$ on one of the three edges of τ due to the continuity condition in the space U^h. Moreover, the problem (5.2) can be solved easily and efficiently because it is defined only locally on a triangle. Next, we define $\boldsymbol{r}_h \in L^2(\Omega)$ such that $\boldsymbol{r}_h|_\tau = \boldsymbol{r}_{h,\tau}$. Finally, we define $\widetilde{\boldsymbol{u}}_h = \boldsymbol{u}_h - \boldsymbol{r}_h$. This vector $\widetilde{\boldsymbol{u}}_h$ is our postprocessed velocity which has better divergence free property and has the same accuracy as the original velocity $\boldsymbol{u}_h$. These results are stated and proved in the following theorem.

THEOREM 5.1. *The vector $\widetilde{\boldsymbol{u}}_h$ is H(div)-conforming and divergence-free in the following sense*

$$\int_{\mathcal{S}(\nu)} q \operatorname{div}_h \widetilde{\boldsymbol{u}}_h \, dx = 0 \tag{5.3}$$

for all $q \in \widehat{P}^h|_{\mathcal{S}(\nu)}$, $\nu \in \mathcal{N}$. Moreover, under the same assumptions in Corollary 4.5 and $\sigma > \frac{1}{2}$, the vector $\widetilde{\boldsymbol{u}}_h$ satisfies the following estimate

$$\|\boldsymbol{u}_h - \widetilde{\boldsymbol{u}}_h\|_{0,\Omega} \le C(h^{\min\{k+1,\sigma+1\}} |\boldsymbol{u}|_{[H^{\min\{k+1,\sigma+1\}}(\Omega)]^2} + \|\boldsymbol{u} - \boldsymbol{u}_h\|_{0,\Omega}). \tag{5.4}$$

Proof. By the first condition of (5.2), it is easy to see that the jump of $\boldsymbol{r}_h$ on each edge e satisfies $[\boldsymbol{r}_h \cdot \boldsymbol{n}] = [\boldsymbol{u}_h \cdot \boldsymbol{n}]$. Thus, the vector $\widetilde{\boldsymbol{u}}_h$ has zero normal jump on each edge. Hence, $\widetilde{\boldsymbol{u}}_h$ is H(div)-conforming. To prove the divergence-free condition (5.3), by definition of $\widetilde{\boldsymbol{u}}_h$, we consider

$$\int_{\mathcal{S}(\nu)} q \operatorname{div}_h \widetilde{\boldsymbol{u}}_h \, dx = \int_{\mathcal{S}(\nu)} q \operatorname{div}_h \boldsymbol{u}_h \, dx - \int_{\mathcal{S}(\nu)} q \operatorname{div}_h \boldsymbol{r}_h \, dx.$$

15

For the first term on the right, we use (5.1) and for the second term on the right, we use Green's identity. We thus obtain that

$$\int_{\mathcal{S}(\nu)} q \operatorname{div}_h \widetilde{\boldsymbol{u}}_h \, dx = \sum_{e \in \mathcal{E}(\nu)} \int_e q[\boldsymbol{u}_h \cdot \boldsymbol{n}] \, d\sigma + \int_{\mathcal{S}(\nu)} \nabla q \cdot \boldsymbol{r}_h \, dx - \sum_{e \in \mathcal{E}(\nu)} \int_e q[\boldsymbol{r}_h \cdot \boldsymbol{n}] \, d\sigma.$$

Since the normal jumps of $\boldsymbol{u}_h$ and $\boldsymbol{r}_h$ are the same and the second condition in (5.2) holds for $\boldsymbol{r}_h|_\tau$, we have

$$\int_{\mathcal{S}(\nu)} q \operatorname{div}_h \widetilde{\boldsymbol{u}}_h \, dx = 0.$$

To prove the estimate (5.4), we note that for each triangle τ, we have

$$\int_\tau |\boldsymbol{r}_{h,\tau}|^2 \, dx \le C h_\tau \sum_{e \subset \partial \tau} \int_e (\boldsymbol{r}_{h,\tau} \cdot \boldsymbol{m})^2 \, d\sigma,$$

where h_τ denotes the diameter of τ. Thus, we have

$$\int_\tau |\boldsymbol{r}_{h,\tau}|^2 \, dx \le C h_\tau \sum_{e \subset \partial \tau} \int_e [\boldsymbol{u}_h \cdot \boldsymbol{n}]^2 \, d\sigma. \tag{5.5}$$

Let $\boldsymbol{u}_h^{(c)}$ be the nodal conforming finite element interpolant of $\boldsymbol{u}$ in the space of piecewise polynomial of degree k with respect to the triangulation $\mathcal{T}$. Since $\boldsymbol{u} \in [H^{1+\sigma}(\Omega)]^2$ and $\sigma > \frac{1}{2}$, this nodal interpolant is well-defined. Then it is well known (c.f. [20]) that $\|\boldsymbol{u} - \boldsymbol{u}^{(c)}\|_{0,\Omega} \le C h^{\min\{k+1,\sigma+1\}} |\boldsymbol{u}|_{[H^{\min\{k+1,\sigma+1\}}(\Omega)]^2}$. Thus summing (5.5) over all τ we obtain that

$$\sum_{\tau \in \mathcal{T}} \int_\tau |\boldsymbol{r}_{h,\tau}|^2 \, dx \le C \sum_{\tau \in \mathcal{T}} h_\tau \sum_{e \subset \partial \tau} \int_e [\boldsymbol{u}_h \cdot \boldsymbol{n}]^2 \, d\sigma$$

$$= C \sum_{\tau \in \mathcal{T}} h_\tau \sum_{e \subset \partial \tau} \int_e [(\boldsymbol{u}_h^{(c)} - \boldsymbol{u}_h) \cdot \boldsymbol{n}]^2 \, d\sigma$$

$$\le C \sum_{\tau \in \mathcal{T}} \int_\tau |\boldsymbol{u}_h^{(c)} - \boldsymbol{u}_h|^2 \, dx$$

$$= C \|\boldsymbol{u}_h^{(c)} - \boldsymbol{u}_h\|_{0,\Omega}^2$$

$$\le C(\|\boldsymbol{u}_h^{(c)} - \boldsymbol{u}\|_{0,\Omega}^2 + \|\boldsymbol{u} - \boldsymbol{u}_h\|_{0,\Omega}^2)$$

$$\le C(h^{\min\{2k+2,2\sigma+2\}} |\boldsymbol{u}|_{[H^{\min\{k+1,\sigma+1\}}(\Omega)]^2}^2 + \|\boldsymbol{u} - \boldsymbol{u}_h\|_{0,\Omega}^2).$$

Hence, we have

$$\|\boldsymbol{u}_h - \widetilde{\boldsymbol{u}}_h\|_{0,\Omega} = \|\boldsymbol{r}_h\|_{0,\Omega} \le C(h^{\min\{k+1,\sigma+1\}} |\boldsymbol{u}|_{[H^{\min\{k+1,\sigma+1\}}(\Omega)]^2} + \|\boldsymbol{u} - \boldsymbol{u}_h\|_{0,\Omega})$$

which proves (5.4).

$\square$

Finally, we remark that a similar divergence free condition is obtained for conforming finite elements [5].

16

6. Numerical results. We start with some numerical tests for our new DG method on two examples. The first is the case when the theoretical solution is given by

$$\boldsymbol{u}_1 = \begin{pmatrix} \pi x^2 (1-x)^2 \sin(2\pi y) \\ -2x(1-x)(1-2x)\sin^2(\pi y) \end{pmatrix},$$
$$p_1 = \sin(x)\cos(y) + (\cos(1) - 1)\sin(1).$$

The computational domain is the square domain $\Omega_1 = (0,1)^2$. These functions are smooth throughout the domain Ω_1.

In the second example, we will test the capability of our method to capture singularities at the reentrant corners on non-convex domains. We consider the L-shaped domain $\Omega_2 = (-1,1)^2 \setminus ([0,1) \times (-1,0])$ with the exact solution given by

$$\boldsymbol{u}_2 = r^\lambda \begin{pmatrix} (1+\lambda)\sin(\varphi)\psi(\varphi) + \cos(\varphi)\psi'(\varphi) \\ -(1+\lambda)\cos(\varphi)\psi(\varphi) + \sin(\varphi)\psi'(\varphi) \end{pmatrix},$$
$$p_2 = -r^{\lambda-1}((1+\lambda)\psi'(\varphi) + \psi'''(\varphi))/(1-\lambda),$$

where

$$\psi(\varphi) = \sin((1+\lambda)\varphi)\cos(\lambda\omega)/(1+\lambda) - \cos((1+\lambda)\varphi)$$
$$- \sin((1-\lambda)\varphi)\cos(\lambda\omega)/(1-\lambda) + \cos((1-\lambda)\varphi),$$

$\lambda \approx 0.54448373678246$ and $\omega = 3\pi/2$. Note that $(\boldsymbol{u}_2, p_2) \in [H^{1+\lambda}(\Omega_2)]^2 \times H^\lambda(\Omega_2)$, cf. [24].

We use piecewise linear elements for the numerical approximations of $\boldsymbol{u}, \boldsymbol{w}, \boldsymbol{z}$ and p, i.e. the case when $k = 1$. In addition, we will also test the performance of the method when the approximation to p is piecewise constant, i.e. $k = 0$. We denote by B the matrix representation of the operators B_h, then B^T is matrix representation of the operators B_h^* because the two discrete operators are adjoint to each other, see Section 2.2. Hence, the second and third equations of (2.16) become

$$B^T u_{h,1} = M\boldsymbol{w}_h,$$
$$B^T u_{h,2} = M\boldsymbol{z}_h,$$

where M is the mass matrix for the space W^h with small diagonal blocks. Hence,

$$\boldsymbol{w}_h = M^{-1}B^T u_{h,1} \text{ and } \boldsymbol{z}_h = M^{-1}B^T u_{h,2}. \tag{6.1}$$

We further denote $\Delta_h = BM^{-1}B^T$, and the matrix representation for b_h to be div_h. After the elimination, the algebraic system for the discrete problem (2.16) is reduced to

$$\begin{pmatrix} \Delta_h & 0 & \text{div}_h^T \\ 0 & \Delta_h & \text{div}_h^T \\ \text{div}_h & 0 & 0 \end{pmatrix} \begin{pmatrix} u_{h,1} \\ u_{h,2} \\ p_h \end{pmatrix} = \begin{pmatrix} f_1 \\ f_2 \\ 0 \end{pmatrix}, \tag{6.2}$$

which consists of two types of unknowns, velocity and pressure. The above linear system is solved for them and then the unknowns for the velocity gradient are calculated from (6.1). We note that the linear system preserves the structure of the Stokes problem and existing domain decomposition algorithms for the Stokes problem can be easily applied for fast solutions, see [25]. The results for the numerical experiments are summarized in Tables 6.1-6.3. In these simulations, the mesh is obtained by first partitioning the domain into an uniform grid and each square in this grid is then divided into two triangles. Using this mesh, the triangulation $\mathcal{T}$ is obtained by the construction outlined

h	$\|e(\boldsymbol{u})\|_0$	order	$\|e(\boldsymbol{u})\|_h$	order	$\|e(p)\|_0$	order	$\|e(\boldsymbol{w}, \boldsymbol{z})\|_0$	order
0.1768	2.46e-03	–	2.67e-01	–	2.08e-02	–	4.29e-02	–
0.0884	6.22e-04	1.99	1.36e-01	0.98	1.03e-02	1.02	1.63e-02	1.40
0.0442	1.56e-04	2.00	6.81e-02	0.99	5.11e-03	1.01	7.30e-03	1.16
0.0221	3.90e-05	2.00	3.41e-02	1.00	2.55e-03	1.00	3.53e-03	1.05
0.0110	9.75e-06	2.00	1.70e-02	1.00	1.27e-03	1.00	1.75e-03	1.01

TABLE 6.1

Convergence for the approximation of $(\boldsymbol{u}_1, p_1)$ on the square domain Ω_1 using $P_1 - P_0$ elements

h	$\|e(\boldsymbol{u})\|_0$	order	$\|e(\boldsymbol{u})\|_h$	order	$\|e(p)\|_0$	order	$\|e(\boldsymbol{w}, \boldsymbol{z})\|_0$	order
0.1768	2.37e-03	–	2.67e-01	–	5.78e-03	–	3.13e-02	–
0.0884	5.97e-04	1.99	1.35e-01	0.98	1.40e-03	2.04	7.99e-03	1.97
0.0442	1.50e-04	2.00	6.79e-02	0.99	3.48e-04	2.01	2.01e-03	1.99
0.0221	3.74e-05	2.00	3.40e-02	1.00	8.65e-05	2.01	5.04e-04	2.00
0.0110	9.35e-06	2.00	1.70e-02	1.00	2.16e-05	2.00	1.26e-04	2.00

TABLE 6.2

Convergence for the approximation of $(\boldsymbol{u}_1, p_1)$ on the square domain Ω_1 using $P_1 - P_1$ elements

h	$\|e(\boldsymbol{u})\|_0$	order	$\|e(\boldsymbol{u})\|_h$	order	$\|e(p)\|_0$	order	$\|e(\boldsymbol{w}, \boldsymbol{z})\|_0$	order
0.5000	5.25e-02	–	1.47e+00	–	8.67e-01	–	1.14e+00	–
0.2500	2.15e-02	1.29	1.01e+00	0.54	5.39e-01	0.69	7.51e-01	0.60
0.1250	9.21e-03	1.22	7.01e-01	0.53	3.51e-01	0.62	5.10e-01	0.56
0.0625	4.08e-03	1.18	4.84e-01	0.53	2.34e-01	0.58	3.49e-01	0.55
0.0312	1.85e-03	1.14	3.33e-01	0.54	1.59e-01	0.56	2.39e-01	0.54

TABLE 6.3

Convergence for the approximation of $(\boldsymbol{u}_2, p_2)$ on the L-shaped domain Ω_2 using $P_1 - P_1$ elements

in Section 2.1. In addition, the refinement of the triangulation $\mathcal{T}$ is based on the refinement of the initial uniform grid. Here we denote h to be the mesh width, i.e. $h := \max_{\tau \in \mathcal{T}} h_\tau$. We also adopt the following conventions: $\|e(\boldsymbol{u})\|_0 = \|\boldsymbol{u} - \boldsymbol{u}_h\|_{0,\Omega}$, $\|e(\boldsymbol{u})\|_h = \|\boldsymbol{u} - \boldsymbol{u}_h\|_h$, $\|e(p)\|_0 = \|p - p_h\|_{0,\Omega}$ and $\|e(\boldsymbol{w}, \boldsymbol{z})\|_0 = \|\boldsymbol{w} - \boldsymbol{w}_h\|_{0,\Omega} + \|\boldsymbol{z} - \boldsymbol{z}_h\|_{0,\Omega}$.

As we can see from Table 6.2, which corresponds to the numerical results for the approximation of the smooth functions $(\boldsymbol{u}_1, p_1)$, the L^2 errors of the velocity, the velocity gradient and the pressure all converge to zero at the rate $\mathcal{O}(h^2)$ asymptotically and the energy errors of the velocity converge to zero at the rate $\mathcal{O}(h)$. These are in full agreement with the estimates in Corollary 4.5 and all the rates are optimal. Moreover, we can use piecewise constant ($k = 0$) approximation instead of piecewise linear approximation for pressure and obtain a stable scheme. The errors and convergence rates for this case are shown in Table 6.1. We see that the order of convergence of L^2 errors is $\mathcal{O}(h)$ for pressure and is $\mathcal{O}(h^2)$ for velocity. Furthermore, the errors in velocity are almost the same as the case when all variables are approximated by piecewise linear polynomials. Thus we can keep the same order of accuracy for velocity even though the approximation degree for pressure is one order lower, and this can help saving the computational cost if velocity is the variable of interest.

On the other hand, for the second example as $\boldsymbol{u}_2 \notin [H^2(\Omega_2)]^2$ and $p_2 \notin H^1(\Omega_2)$, the corresponding convergence rates are affected by the regularity of these functions. We observe from Table 6.3 that the orders of convergence of $\|e(\boldsymbol{u})\|_h$, $\|e(p)\|_0$ and $\|e(\boldsymbol{w}, \boldsymbol{z})\|_0$ in the second example are likely to approach λ, as predicted by Corollary 4.5. The convergence of L^2 errors of $\boldsymbol{u}_2$ does not follow

18

that in Corollary 4.5 since $\boldsymbol{u}_2$ is no longer in $[H^2(\Omega)]^2$. We remark that similar results are also observed in [24].

Next, we will numerically illustrate how well the divergence free condition is satisfied by the numerical solution. In Table 6.4 and Table 6.5, we present the L^∞-norm of the divergence of $\boldsymbol{u}_h$ for the examples shown above. For the case with smooth solution, that is $\boldsymbol{u}_1$, we see from Table 6.4 that the L^∞ error of the divergence of $\boldsymbol{u}_h$ converges linearly with the mesh sizes for both the $P_1 - P_0$ and the $P_1 - P_1$ elements. For the case with singular solution, that is $\boldsymbol{u}_2$, we see from Table 6.5 that the L^∞ error of the divergence of $\boldsymbol{u}_h$ has no convergence. In fact, for this example, the error mainly comes from the corner singularity. In FIG. 6.1, the divergence of $\boldsymbol{u}_h$ is shown and we see clearly that large error occurs near the corner.

h	$\|\mathrm{div}_h\boldsymbol{u}\|_{L^\infty(\Omega)}$ with $P_1 - P_0$	order	$\|\mathrm{div}_h\boldsymbol{u}\|_{L^\infty(\Omega)}$ with $P_1 - P_1$	order
0.3536	8.43e-01	–	7.86e-01	–
0.1768	5.12e-01	0.72	4.87e-01	0.69
0.0884	2.86e-01	0.84	2.75e-01	0.82
0.0442	1.49e-01	0.94	1.44e-01	0.94
0.0221	7.59e-02	0.97	7.35e-02	0.97

TABLE 6.4

L^∞-norm of $div_h\boldsymbol{u}_h$ for the example with solution $(\boldsymbol{u}_1, p_1)$ on the square domain Ω_1 using $P_1 - P_0$ and $P_1 - P_1$ elements

h	$\|\mathrm{div}_h\boldsymbol{u}\|_{L^\infty(\Omega)}$	order
0.5000	1.45e-00	–
0.2500	1.75e-00	-0.27
0.1250	2.41e-00	-0.46
0.0625	3.31e-00	-0.46
0.0312	4.55e-00	-0.46

TABLE 6.5

L^∞-norm of $div_h\boldsymbol{u}_h$ for the example with singular solution $(\boldsymbol{u}_2, p_2)$ on the L-shaped domain Ω_2 using $P_1 - P_1$ elements

FIG. 6.1. The divergence of $\boldsymbol{u}_h$ for the example with singular solution $(\boldsymbol{u}_2, p_2)$ on the L-shaped domain Ω_2 using $P_1 - P_1$ elements

19
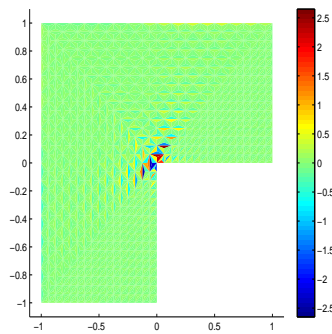
We will now present results for the postprocessed velocity $\widetilde{\boldsymbol{u}}_h$. In Table 6.6 and Table 6.7, the L^2 errors of the postprocessed velocity $\widetilde{\boldsymbol{u}}_h$ are shown for various mesh sizes for the example with the smooth solution $(\boldsymbol{u}_1, p_1)$, and in Table 6.8, the L^2 errors of the postprocessed velocity $\widetilde{\boldsymbol{u}}_h$ are shown for various mesh sizes for the example with the singular solution $(\boldsymbol{u}_2, p_2)$. From these results, we see that the error of $\widetilde{\boldsymbol{u}}_h$ has the same order of accuracy as $\boldsymbol{u}_h$. Regarding the divergence free condition (5.3), we will take $q = 1$ on each $\mathcal{S}(\nu)$ and present the maximum of $\int_{\mathcal{S}(\nu)} \mathrm{div}_h \widetilde{\boldsymbol{u}}_h$ over the whole domain in Table 6.6 and Table 6.7 for $(\boldsymbol{u}_1, p_1)$ and in Table 6.8 for $(\boldsymbol{u}_2, p_2)$. The results for other choices of q are the same and we skip the repetition. In addition, the values of $\int_{\mathcal{S}(\nu)} \mathrm{div}_h \widetilde{\boldsymbol{u}}_h$ over the whole domain are shown in FIG. 6.2 and FIG. 6.3 for $(\boldsymbol{u}_1, p_1)$ and $(\boldsymbol{u}_2, p_2)$ respectively. From these results, we see that the value of $\int_{\mathcal{S}(\nu)} \mathrm{div}_h \widetilde{\boldsymbol{u}}_h$ is zero up to the machine precision.

h	$\|\boldsymbol{u} - \widetilde{\boldsymbol{u}}_h\|_{0,\Omega}$	order	$\max \left| \int_{\mathcal{S}(\nu)} \mathrm{div}_h \widetilde{\boldsymbol{u}}_h \right|$
0.3536	1.47e-02	–	3.09e-16
0.1768	3.97e-03	1.89	8.38e-16
0.0884	1.01e-03	1.97	1.39e-15
0.0442	2.54e-04	1.99	1.55e-15
0.0221	6.37e-05	2.00	2.18e-15

TABLE 6.6

Convergence of $\widetilde{\boldsymbol{u}}_h$ for the approximation of $(\boldsymbol{u}_1, p_1)$ on the square domain Ω_1 using $P_1 - P_0$ elements

h	$\|\boldsymbol{u} - \widetilde{\boldsymbol{u}}_h\|_{0,\Omega}$	order	$\max \left| \int_{\mathcal{S}(\nu)} \mathrm{div}_h \widetilde{\boldsymbol{u}}_h \right|$
0.3536	1.44e-02	–	7.06e-16
0.1768	3.91e-03	1.88	9.66e-16
0.0884	9.96e-04	1.97	1.19e-15
0.0442	2.50e-04	1.99	2.06e-15
0.0221	6.26e-05	2.00	6.75e-15

TABLE 6.7

Convergence of $\widetilde{\boldsymbol{u}}_h$ for the approximation of $(\boldsymbol{u}_1, p_1)$ on the square domain Ω_1 using $P_1 - P_1$ elements
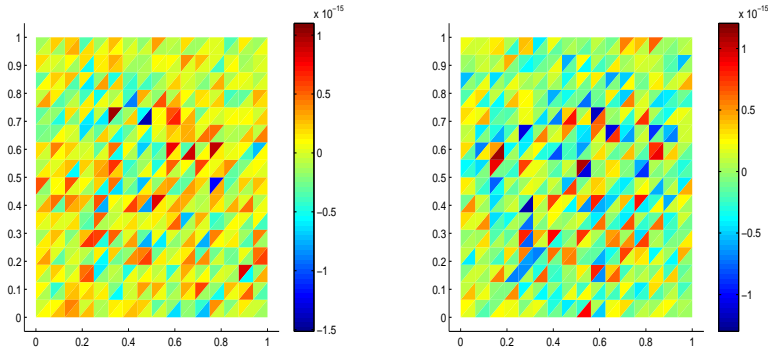
FIG. 6.2. *The value of $\int_{\mathcal{S}(\nu)} \mathrm{div}_h \widetilde{\boldsymbol{u}}_h$ for the example with solution $(\boldsymbol{u}_1, p_1)$ on the square domain Ω_1 using $P_1 - P_0$ (left) and $P_1 - P_1$ (right) elements*

h	$\|\boldsymbol{u} - \widetilde{\boldsymbol{u}}_h\|_{0,\Omega}$	order	$\max\left|\int_{\mathcal{S}(\nu)} \mathrm{div}_h \widetilde{\boldsymbol{u}}_h\right|$
0.5000	6.31e-02	–	4.29e-15
0.2500	2.52e-02	1.33	3.65e-15
0.1250	1.03e-02	1.29	2.78e-15
0.0625	4.39e-03	1.23	5.05e-15
0.0313	1.93e-03	1.18	2.72e-15

TABLE 6.8

Convergence of $\widetilde{\boldsymbol{u}}_h$ for the approximation of singular solution $(\boldsymbol{u}_2, p_2)$ on the L-shaped domain Ω_2 using $P_1 - P_1$ elements
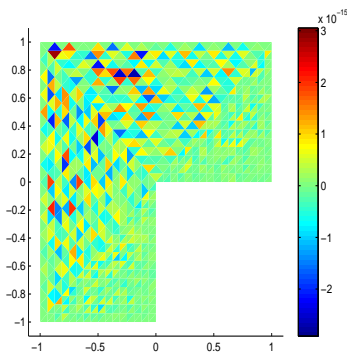
FIG. 6.3. *The value of $\int_{\mathcal{S}(\nu)} div_h \widetilde{\boldsymbol{u}}_h$ for the example with singular solution $(\boldsymbol{u}_2, p_2)$ on the L-shaped domain Ω_2 using $P_1 - P_1$ elements*

7. Conclusion. In this paper, we develop and analyze a staggered DG method for the Stokes system. Our method shares the same advantages of existing staggered grid-based methodologies and provides a more practical tool for problems that require higher order accuracy and triangular meshes. The staggered property naturally gives inter-element flux terms so that numerical fluxes or penalty parameters are not needed. One distinctive feature of our method is that all variables are approximated by the same order of polynomial, and optimal orders of convergence in both L^2 and energy norms are proved. Another feature of our method is that the approximation degree of pressure can be taken one order lower than velocity, without affecting the accuracy of the velocity and the stability of the method, in order to reduce the computational cost. A superconvergence result is also obtained, namely, the error of the velocity in the energy norm is one order higher when the error is computed as the difference between the numerical solution and the interpolant into the new DG space. To enhance divergence free property of the numerical velocity, we propose a local postprocessing technique. The postprocessed velocity retains the original accuracy and is locally divergence free, in the sense that the elementwise integral of the product of the divergence and any test function in the pressure space is zero. Numerical results are shown to confirm these estimates and the ability to capture singular solutions.

REFERENCES

[1] D. ARNOLD, J. QIN, *Quadratic velocity/linear pressure Stokes elements*, Advances in Computer Methods for Partial Differential Equations-VII, IMACS, 1992, pp. 28–34.
[2] P. BLANC, R. EYMARD, R. HERBIN, *A staggered finite volume scheme on general meshes for the generalized*

       Stokes problem in two space dimensions, International Journal on Finite Volumes, 2 (2005), pp. 1–31.

[3] B. J. BOERSMA, *A staggered compact finite difference formulation for the compressible Navier-Stokes equations*, J. Comput. Phys., 208 (2005), pp. 675–690.

[4] D. BOFFI, F. BREZZI, M. FORTIN, *Finite elements for the Stokes problem*, Mixed finite elements, compatibility conditions, and applications, Lectures given at the C.I.M.E. Summer School held in Cetraro, Italy, June 26-July 1, 2006, Lecture Notes in Mathematics, Springer Verlag, 1939, pp. 45–100.

[5] D. BOFFI, N. CAVALLINI, F. GARDINI, L. GASTALDI, *Local mass conservation of Stokes finite elements*, J. Sci. Comput., 52 (2012), pp. 383–400.

[6] D. BRAESS, *Finite elements. Theory, fast solvers, and applications in elasticity theory*, Cambridge University Press, Cambridge, 2007.

[7] S. C. BRENNER, *Poincaré-Friedrichs inequalities for piecewise H^1 functions*, SIAM J. Numer. Anal., 41 (2003), pp. 306–324.

[8] J. CARRERO, B. COCKBURN, D. SCHÖTZAU, *Hybridized globally divergence-free LDG methods. Part I: The Stokes problem*, Math. Comput., 75 (2005), pp. 533–563.

[9] B. COCKBURN, J. GOPALAKRISHNAN, N.C. NGUYEN, J. PERAIRE, F.-J. SAYAS, *Analysis of an HDG method for Stokes flow*, Math. Comput., 80 (2011), pp. 723–760.

[10] B. COCKBURN, G. KANSCHAT, D. SCHÖTZAU, *A locally conservative LDG method for the incompressible Navier-Stokes equations*, Math. Comp., 74 (2005), pp. 1067–1095.

[11] B. COCKBURN, G. KANSCHAT, D. SCHÖTZAU, C. SCHWAB, *Local discontinuous Galerkin methods for the Stokes system*, SIAM J. Numer. Anal., 40 (2002), pp. 319–343.

[12] E. T. CHUNG, P. CIARLET, *A staggered discontinuous Galerkin method for wave propagation in media with dielectrics and meta-materials*, J. Comput. Appl. Math., 239 (2013), pp. 189–207.

[13] E. T. CHUNG, P. CIARLET, T. F. YU, *Convergence and superconvergence of staggered discontinuous Galerkin methods for the three-dimensional Maxwell's equations on Cartesian grids*, J. Comput. Phys., 235 (2013), pp. 14–31.

[14] E. T. CHUNG, Q. DU, J. ZOU, *Convergence analysis on a finite volume method for Maxwell's equations in non-homogeneous media*, SIAM J. Numer. Anal., 41 (2003), pp. 37–63.

[15] E. T. CHUNG, B. ENGQUIST, *Convergence analysis of fully discrete finite volume methods for Maxwell's equations in nonhomogeneous media*, SIAM J. Numer. Anal., 43 (2005), pp. 303–317.

[16] E. T. CHUNG, B. ENGQUIST, *Optimal discontinuous Galerkin methods for wave propagation*, SIAM J. Numer. Anal., 44 (2006), pp. 2131–2158.

[17] E. T. CHUNG, B. ENGQUIST, *Optimal discontinuous Galerkin methods for the acoustic wave equation in higher dimensions*, SIAM J. Numer. Anal., 47 (2009), pp. 3820–3848.

[18] E. T. CHUNG, C. S. LEE, *A staggered discontinuous Galerkin method for the curl-curl operator*, IMA J. Numer. Anal., 32 (2012), pp. 1241–1265.

[19] E. T. CHUNG, C. S. LEE, *A staggered discontinuous Galerkin method for the convection-diffusion equation*, J. Numer. Math., 20 (2012), pp. 1–31.

[20] P. CIARLET, *The Finite Element Method for Elliptic Problems*, North-Holland, Amsterdam.

[21] V. GIRAULT, P.-A. RAVIART, *Finite element approximation of the Navier-Stokes equations*, Lecture Notes in Mathematics, Springer-Verlag, Berlin, 749.

[22] J. GOPALAKRISHNAN, J. GUZMAN, *A second elasticity element using the matrix bubble*, IMA J. Numer. Anal., 32 (2012), pp. 352–372.

[23] F. H. HARLOW, J. E. WELCH, *Numerical calculation of time-dependent viscous incompressible flow of fluid with a free surface*, Phys. Fluids, 8 (1965), pp. 2182–2189.

[24] P. HOUSTON, D. SCHÖTZAU, X. WEI, *A mixed DG method for linearized incompressible magnetohydrodynamics*, J. Sci. Comp., 40 (2009), pp. 281–314.

[25] H. H. KIM, E. T. CHUNG, C. S. LEE, *FETI-DP preconditioners for a staggered discontinuous Galerkin formulation of the two-dimensional Stokes problem*, Submitted.

[26] D. SCHÖTZAU, C. SCHWAB, A. TOSELLI, *Mixed hp-DGFEM for incompressible flows*, SIAM J. Numer. Anal., 40 (2003), pp. 2171–2194.

[27] D. SCHÖTZAU, T. WIHLER, *Exponential convergence of mixed hp-DGFEM for Stokes flow in polygons*, Numer. Math., 96 (2003), pp. 339–361.